Thin-Film Sensor-Integrated Smart Cutting Tools for Real-Time Machining Temperature Measurement in Industry 4.0

Sathishkumar *Selvan*[1], Karthikeyan *Ravichandran*[2], Viswanathan *Nallasamy*[3], Thirumoorthy *Kumarasami Annamalai*[4], Chacko *Jose*[5], Nanthakumar *Sivasamy*[6], and Girimurugan *Ramasamy*[7*]

[1]Department of Mechanical Engineering, Shree Venkateshwara Hi-Tech Engineering College, Gobichettipalayam 638455, Tamil Nadu, India
[2]Department of Automobile Engineering, Rajalakshmi Engineering College, Chennai 602105, Tamil Nadu, India
[3,7]Department of Mechanical Engineering, Nandha College of Technology, Perundurai 638052, Tamil Nadu, India.
[4]Department of Naval Architecture and Offshore Engineering, Academy of Meritime Education and Training, Chennai 603112, Tamil Nadu, India
[5]Retired Principal, St Aloysius College, Thrissur 680611, Kerala, India
[6]Department of Mechanical Engineering, PSG Institute of Technology and Applied Research, Coimbatore 641062, Tamil Nadu, India

Abstract. This research delves into the incorporation of thin-film sensors made of zirconium aluminum nitride (ZrAlN) and titanium aluminum nitride (TiAlN) into cutting tools to track the temperature of Ti6Al4V titanium alloy as it is being machined in real-time. The sensors were calibrated for temperatures up to 750°C and then deposited directly onto the surfaces of the tools. The coatings included many layers that served to shield the tools from electrical currents and wear. The sensors show varying β sensitivities spanning a temperature range of 928 to 6680 K for ZrAlN and from 112 to 825 K for TiAlN, as a result of being integrated into the multilayer coating. Cutting temperature was found to be affected by cutting conditions, feed rate, depth of cut, and cooling, according to cutting tests performed under different cutting settings. Our research shows that determining the cutting temperature relies heavily on where the sensor is located on the tool's rake face. In a "plug-and-play" form that is compatible with industry standards, the study presents a new tool connector that allows for the integration and signal retrieval of the cutting tool. Smart cutting tools enable real-time, in-situ temperature monitoring by wireless transfer, supporting Industry 4.0 integration in modern manufacturing.

[*]Corresponding Author: dr.r.girimurugan@gmail.com

1 Introduction

To enhance and progress of cutting processes, tool condition monitoring were essential and tool failures of 20% of machine downtimes. This study addresses the challenge of tool wear in Ti6Al4V thin-walled machining by integrating domain knowledge into a data-driven monitoring framework. By filtering weak signal features linked to cutting force and axial bending moments, the approach enhances real-time recognition of wear conditions, improving accuracy by 7% while reducing parameters, laying a foundation for Industry 4.0 digital twin applications [1]. Using acoustic emission sensors during titanium alloy turning, this work evaluates classification methods for tool and machine state monitoring. By extracting and refining features like Fourier and mel-frequency coefficients, quadratic discriminant analysis achieved 98.6% accuracy, highlighting the potential of AE-based monitoring to support Industry 4.0 cutting tool applications [2]. A GSOM-based unsupervised AI framework with real-time specific force coefficient estimation was developed for titanium alloy cutting. Compared with traditional control charts, this approach achieved a 13.2% RMSPE, robustly detecting tool end-of-life under variable lubrication and speed, supporting reliable Industry 4.0 tool condition monitoring [3]. This work proposes an unsupervised method for Ti6Al4V milling tool wear monitoring by estimating specific force coefficients through a mechanistic model. Validated across machines and lubrication types, the approach used control charts and principal component regression to detect notch wear and chipping, offering robust industrial monitoring aligned with Industry 4.0 demands [4]. Interrupted milling Inconel 718 with TiAlN/NbN carbide inserts was monitored using imagery signals processed through multi-sectional SVD. This approach enhanced feature extraction under complex wear morphology, enabling machine learning to predict flank wear with only 2.36% error and optimize cutting conditions for extended tool life in harsh machining [5]. ZrAlN thin films were developed by magnetron sputtering for high-temperature thermistor use in cutting tool coatings. Integrated into multilayers with Arduino® signal acquisition, the ZrO_7, AlO_3N layer provided accurate real-time temperature sensing up to 400°C with 7% error, demonstrating strong potential for Industry 4.0 smart machining and wear shielding [6]. Machine learning regression models were applied to predict Permanent Magnet Synchronous Motor temperatures, eliminating costly direct sensing. The KNN regressor achieved 98.72% test accuracy, enabling low-cost monitoring of electrical machinery, improving efficiency and safety in Industry 4.0 systems [7]. A blade-coated Ag-RTD array was fabricated directly on quartz rings for tube furnace monitoring in material synthesis. With high TCR (2854 ppm/°C) and accuracy (1.8% FS), the system enabled precise real-time temperature mapping up to 600 °C, advancing furnace-based titanium alloy and alloy sintering processes [8]. SiBCN ceramic-based sensors were developed as high-temperature NTC thermistors, showing sensitivity up to 980 °C with B-values of 3118 K. Compared to thermocouples authors demonstrated faster response and high stability, enabling durable real-time monitoring in harsh machining and aerospace environments [9]. A rotational vibration energy harvester using Fe-Ga alloy was designed to power wireless temperature sensors in rotating carriers. By exploiting centrifugal softening and magneto strictive effects, it achieved 22.86% energy efficiency and supported real-time temperature monitoring in low-power Industry 4.0 applications [10]. Considering the limitations stated in the literature, this study proposes a solution with a particular emphasis on cutting titanium alloys. A comprehensive approach which includes the following to achieve this goal: (i) use a multilayer coating of complete nitride that was created using a single magnetron sputtering machine; this coating would include temperature sensors made of zirconium aluminum nitride (ZrAlN) and titanium aluminum nitride (TiAlN) that had been produced in earlier research; (ii) It is crucial to calibrate the multilayer coating up to 750°C because titanium alloys are typically machined

at high temperatures. (iii) To retrieve the signal from the sensor while keeping the tool holder robust and traditionally used in industrial settings, a modified tool holder is used. (iv) Orthogonal cutting are performed at Ti6Al4V alloys to determine which cutting parameters had impact at cutting temperatures. and no one has ever used thin-film sensors for an analysis like this before. Finally, by making wireless transmission by Arduino platform, we show how easy it is to combine the thin-film by traditional electronics. By demonstrating ease of integration of smart cutting tools as contemporary, automated manufacturing environments, this component seeks to validate the systems with Industry 4.

2 Experimental Methods

2.1 Sensor-Calibrated Cutting Temperature Setup

A Gurutzpe 15 kW lathe a mounted tool holder and a Data Sync module that sends temperature readings to a personal computer by Bluetooth (1) with a particular connector used to securely attach the multilayer-coated cutting tool and retrieve its electrical signal. The electrical contacts were shielded from dangerous cutting environment by this connector, which was 3D printed in 306 stainless steel using selective laser sintering (SLS). Connecting cutting tool to Data Sync module, connector lets cables go by inner channels. Without altering its primary features, the SECO® tool holder CSSPR2525 had adjusted to fit connector. In addition to preserving the cutting tool insert's "plug-and-play" mechanism, this design makes it possible to handle the tool holder in accordance with standard industrial practice. There are two insulator films made of AlN, one with a thickness of 1000 nm and the other of 600 nm, between TiAlN and ZrAlN active layers. To enhance wear resistance, entire structure were coated by TiAlN. Two zirconium/titanium targets and two aluminum targets were arranged at closed-field magnetic within a single magnetron sputtering device to apply multilayer coating. With exception of ZrAlN layer, all of the process steps and parameters have been previously described in detail in the literature. A nitrogen-argon gas mixture with a ratio of 1.6 was used to carry out the deposition process at a working pressure of about 0.25 Pa. One revolution per minute (RPM) was kept for the table and five rpm for the satellite. Aluminum had its power densities set at around 1.9 $W \cdot cm^{-2}$ using two sources, whereas zirconium had theirs set at 5.5 $W \cdot cm^{-2}$ using the same two sources. The negative bias applied to the substrate was 40 V, while the positive bias pulse frequency was 250 kHz and the reverse time was 0.5 μs. Deposition process lasted for 60 minutes, during which the gap between the target and substrate was maintained at 100 mm. The substrate temperature was kept at around 200 °C during the whole process. The two-point measurement (2PM) approach was used to assess the electrical resistance fluctuation of the multilayer coating as a function of temperature. As part of the calibration procedure, the temperature was subjected to four cycles, rising from room temperature to 750°C at a rate of approximately 20°C per minute, followed by cooling by natural means. A high-resolution multimeter was used to measure the electrical resistance (acquisition frequency: 10 Hz). Then, data were fitted by Eq. (1), taking into account room temperature resistance value (R25). The multilayer structure's sensor layers were calibrated in a vacuum environment with a relative humidity of 5% Ar/H_2. This was done to avoid oxidation of the tungsten carbide (WC) substrate and titanium nitride (TiN) contacts, assuring operational stability and performance. Over a specified temperature range (50-200ºC), the thermistor sensitivity index β was determined using:

$$\beta_{[50-200°C]} = \frac{\ln\left(\frac{R_{T1}}{R_{T2}}\right)}{\left(\frac{1}{T_1}-\frac{1}{T_2}\right)} \quad (1)$$

The electrical resistances at temperatures T1 and T2 are represented as RT1 and RT2, respectively, in Eq. (1), with β given in Kelvin. The connections inside the Data Sync module, which sends temperature data to the 33BLE connected to PC. With 33IoT serving as its peripheral, the 33BLE takes center stage. A 10kΩ variable resistor is used setpoint tuning of TiAlN, and a Rail-to-Rail Input/Output is used as signal amplification. Prior research has verified that signal amplification is necessary due to the TiAlN system's lower β value compared to the ZrAlN. The electronic system was powered by a 3.7 V battery and had resistors designed to amplify about ten times. The sensor and the 10kΩ variable resistor were connected through a voltage divider to acquire the temperature. In order to get the temperature (T) in Kelvin, we used Eq. (2):

$$T = \frac{RT \cdot \beta}{\left(RT \cdot \log\frac{Rsensor}{R25} + \beta\right)} \quad (2)$$

Equation (2) finds the values of RT, Rsensor, and R25; the sensitivity of the thermistor, denoted as ϋ is derived from Equation (1). In the Arduino IDE (C++), the cutting tool temperature was calculated using Eq. (2). To deal with tool-to-tool variation in R25, two analog input ports on the Arduino were utilized. A divider is used by Analog A0 to measure the value of the variable resistor, which is 10 kΩ, in relation to a fixed 10 kΩ resistor that is set in the IDE. Using voltage divider connected to variable resistor and sensor (with a pre-stored value), Analog A2 determines the voltage. With this setup, the temperature readings are always accurate because R25 is automatically calculated and stored whenever the sensor is attached. According to Eq. (2), at room temperature, R25 should be quite close to Rsensor. When the ZrAlN sensor is linked, analog input A1 is not utilized; however, when TiAlN sensor is attached extract sensor resistance. In order to confirm the correctness and dependability of Bluetooth signal, particularly for TiAlN sensor, the multilayer coating was subjected to additional testing after the calibration, this time in a vacuum, at constant temperatures of 100 and 200°Cfor 10 minutes. For every experiment, a 100 ms acquisition rate was utilized.

$$\beta_{[50-20\ °C]} = \frac{\ln\left(\frac{R_{T1}}{R_{T2}}\right)}{\left(\frac{1}{T_1} - \frac{1}{T_2}\right)} \quad (3)$$

Electrical resistance at temperatures T_1. and T_2. are represented by, R_{T1}. and, R_{T2}. In Eq. (1), β is in K. A 10kΩ resistor is used setpoint tuning of TiAlN system and a Rail-to-Rail Input/Output is used as signal amplification. Prior research has verified that micro flown sound sensor was used for real-time tool wear monitoring in SAE 1015 steel machining with uncoated, TiAlN, and TiAlN/WC-C inserts. By correlating flank wear with i-kaz coefficients and validating with neural networks (error 3.7e−5), the system effectively predicted wear progression, supporting Industry 4.0 online monitoring [11]. The electronic system was powered by a 3.7 V battery and had resistors designed to amplify about ten times. The sensor and the 10kΩ variable resistor were connected through a voltage divider to acquire the temperature. In order to get the temperature (T) in Kelvin, Eq. (2) was used:

$$T = \frac{RT \cdot \beta}{\left(RT \cdot \log\frac{Rsensor}{R25} + \beta\right)} \quad (4)$$

Equation (2) uses the abbreviations RT, Rsensor, and R25 to represent various variables: room temperature (K), sensor resistance (Ω), and resistance at room temperature (Ω). The sensitivity β of the thermistor is determined using Eq. (1). The cutting tool's temperature was returned using Eq. (4), which was programmed in C++ within the Arduino IDE. Using a voltage divider connected to sensor and a resistor (with a pre-stored value). Analog A2 determines the voltage. With this setup, the temperature readings are always accurate because R25 is automatically calculated and stored whenever the sensor is attached. According to Eq. (4), at room temperature, R25 should be quite close to Rsensor.

Although the ZrAlN sensor does not make use of analog input A1 when connected, the TiAlN sensor does read voltage from OpAmp to determine sensor resistance. In order to confirm correctness and dependability of Bluetooth signal, particularly for TiAlN sensor, the multilayer coating was subjected to additional testing after the calibration, this time in a vacuum at constant temperatures of 100 and 200°C for 10 minutes. For every experiment, a 100 ms acquisition rate was utilized.

2.2 Turning Parameters and Surface Characterization of Ti6Al4V Alloy

The workpiece of 55 mm in length and 80 mm diameter was subjected to cutting tests using the SPGN120308 CP200 tool according to settings established per SECO® recommendations, with nose radius of 0.8 mm. These guidelines state that the cutting speed (Vc) should be between 25 and 44 m/min, depth of cut (ap) should be between 0.21 and 1.93 mm, and the feed rate should be between 0.21 and 0.39 mm/rev. Cutting at a speed of 35 m/min, feed rate 0.12 mm/rev, and depth cut of 1 mm was parameters used for the initial cut. Six small grooves, 3 mm at length and 0.3 mm at depth, with around 5 mm of space between them, were cut into the workpiece to ensure the system's responsiveness. Machining parameters for titanium alloy are shown in Table 1. Conditions 1-6 examined the effects of varied feed rates, while conditions 1-3 tested the effects of changing depth of cut. Condition 9 looked at how moderate cooling affected cutting edge, cutting coolant a metalworking soluble fluid that was 6% concentrated in water. As a last step, the impact of cutting speed was evaluated by comparing conditions 1 and 10.

Table 1. Machining parameters for Ti6Al4V

f (mm/rev)	a_p(mm)	Average V_c (m/min)
0.121	2.0	42
	2. 5	
	2.25	
0.312	2.5	
	2.0	
	2.0	
	2.25	
	1.5	
	1.5	
0.331	2.5	80

To ensure the ZrAlN sensor could be reliably used in future tests, conditions 3, 6, and 8 were re-tested. Additionally, under test conditions 8, the TiAlN and ZrAlN sensors' performances were contrasted. The following calculation was used to compute the lathe is rotating speed (n):

$$n = \frac{V_c \cdot 1000}{(\pi \cdot D)} \quad (5)$$

The variables n in Eq. (5) are rotations per minute (rpm), Vc in m/min, D in millimeters (mm) for the workpiece diameter. Utilizing confocal microscope that offers precise surface profiles, the topography of the tool rake faces at cutting edge was examined.

Tool fitted with TiAlN sensor underwent this examination both prior to and after to the cutting trials. In order to compare the surface degradation rates, the ZrAlN sensor instrument was also used.

3 Results and Discussions

3.1 Zraln and Tialn Calibration

For precise temperature readings during cutting tests, it is necessary to calibrate the ZrAlN and TiAlN sensors. To prevent the shadow mask made of polyimide tape from coming loose while the sensors were being deposited, they were both placed within 1 mm of the cutting edge. By tuning Al^+ ion energy, stable cubic NaCl-structure phases were achieved, enhancing high-temperature resistance for cutting tool coatings, supporting thin-film TiAlN/ZrAlN applications in real-time monitoring and advanced Industry 4.0 machining [12]. Each material has its own unique sensor architecture; for example, ZrAlN sensors are square and TiAlN sensors are meandering. Due to the fact that ZrAlN has a higher resistivity than TiAlN, a meander structure would add complexity to the acquisition system and the sensor's resistance without being necessary.

3.2 Temperature Sensitivity and Performance of Sensors

Log resistance vs. temperature and multilayer coating with TiAlN (a) and ZrAlN (b) sensors are shown in Fig. 1. Following the method described in a recent work, the two cutting tools were subjected to thermal annealing in a vacuum for 20 minutes at 400°C. The expected behavior of both sensors, a decrease in resistance with increasing temperature, is exhibited by semiconductors. The values published in the literature for these films are consistent with the calculated sensitivity β values of 112.4 K for the TiAlN layer and 928.6 K for the ZrAlN layer. Although the behavior and sensitivity levels of the semiconductors are in agreement with predictions and earlier research, we do admit that our stabilizing process is a methodological restriction. Although 400°C is ideal for annealing according to earlier research, it is much lower than the temperatures used for calibration, which can reach as high as 750°C. While the sensors' ability to return to their original resistance during cycling testing indicates stability under short exposures to high temperatures, it has to be seen whether this stability holds up under longer periods of high temperatures. Fig. 1(a) shows that average measured up to 400°C are well-aligned with β fit for TiAlN sensor. Above 400°C, however, there is a noticeable drop in resistance, and data provide large deviation from fitting. At 300°C, β fit begins to vary slightly, but otherwise, the ZrAlN sensor (refer to Fig. 1(b)) exhibits a comparable pattern of behavior. Both sensors are rather complicated to calibrate, yet they show comparable reactions and repeatability. In the region of 400-600°C, the sensitivity of TiAlN is 802.7± 115.6 K and that of ZrAlN is 6423.4 ± 521.8 K, respectively.

3.3 Stability Analysis with Arduino-Based Data Acquisition

Combining β values from segments or using a polynomial/exponential non-linear fit are necessary steps in developing a full-range calibration model, as illustrated at Fig. 1(a) and Fig. 1(b). R25 differs marginally across materials of the same type and substantially between TiAlN and ZrAlN, as previously indicated.

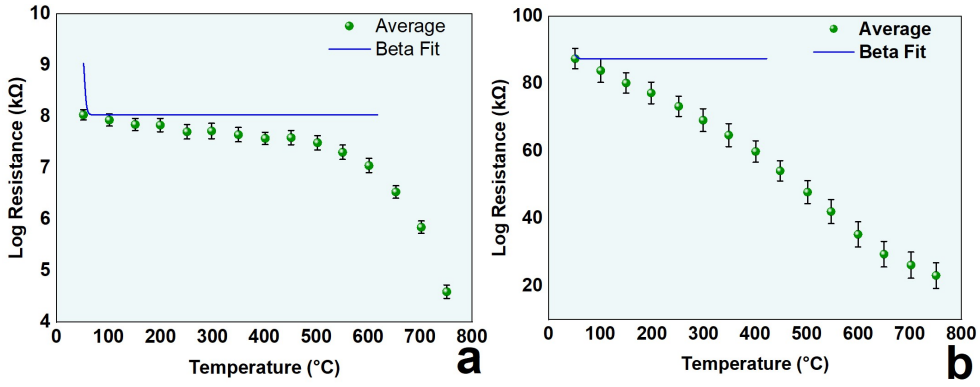

Fig. 1. Calibration TiAlN (a) ZrAlN (b) sensors from β-fit over 4 heating–cooling cycles to 750°C

This goes beyond what our study can cover because it requires a sophisticated calibrating method. In Eqn. (2) of Arduino IDE, we used beta fit as calibration model for sensors because it is suitable up to 400°C.When amplified, TiAlN sensor can accomplish ~0.18°C/step with 12-bit ADC of the Arduino, whereas when unamplified, it can achieve ~0.28 °C/step. Signal stability and cycling performance were assessed during the tests, which ranged from 100 to 420°C. One can see the signal being adjusted to coincide with the initial temperature reading from the reference thermocouple (TC) in Figure 2(a) and (b). On display in Figure 2(a) is a single heating-cooling cycle featuring 10-minute holds at 100 and 220°C. The TiAlN sensor's temperature readings show excellent agreement and stability with the TC readings. These minor discrepancies are caused by the initial tuning that was done when β function was used for calibration. Figure 2(b) shows temperature response within a range of 300 to 420°C as measured during several heating-cooling cycles. Repeated cycles reveal no change in the sensor's accuracy or stability, and it stays in tight alignment with the TC. An Arduino-based infrared temperature measurement system was implemented for CNC milling of aluminum alloys. The setup matched the accuracy of a Fluke Ti400 while enabling continuous real-time monitoring and data logging, expanding smart machining integration under Industry 4.0 as observed in previous studies [13]. Taken as a whole, the data shows that the system can reliably monitor temperature changes and report them at regular intervals. This tight agreement with the TC proves that the sensor is accurate and dependable. Thermal inertia and discrepancies in sensor reaction times (the thin-film sensor 9.6 s and the thermocouple 8.7 s) are likely to responsible for the small delay seen in Fig. 2(b). The TC demonstrates a more rapid drop in temperature as the cooling stages progress. The results show that the calibration, which used the β function, was effective for both sensors up to 420°C in the cutting trials.

3.4 TiaIn-Based Cutting Temperature Measurement

Fig. 3 shows the temperature profile following the initial titanium alloy cutting test using the TiAlN sensor. The image depicts the thermal dynamics, drawing attention to important parts of the cutting procedure. A quick rise in temperature begins when the cutting tool makes contact with the workpiece material. Plastic and friction deformation at tool-workpiece interface are responsible for this first rise. Upon initial rise to approximately 70-120°C, the temperature begins to rise more slowly, suggesting a quasi-steady-state situation.

Even though the temperature is still going up, the temperature curve's slope is much smaller than it was in the beginning, which means that the rates of heat generation and dissipation are almost equal but not quite there yet. As the tool slides across the finely grooved surface of the workpiece, momentarily decreasing the ap, the temperature changes at regular intervals reflect this.

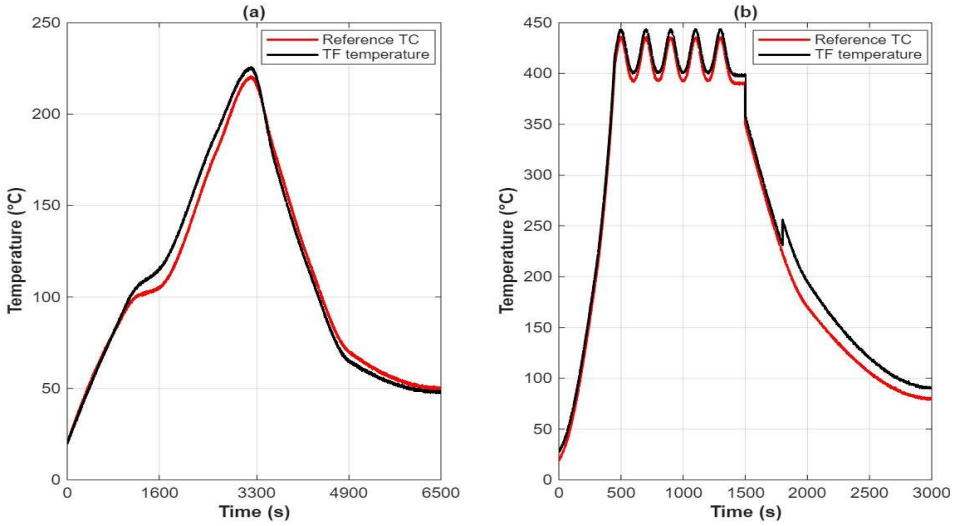

Fig. 2. Heating–cooling tests of TiAlN multilayer in vacuum: (a) 100–200 °C stability; (b) 300–400 °C cycling

The quick decrease in temperature as the tool is disengaged for around 300 seconds demonstrates the sensor's high sensitivity, as shown by its intermittent behavior. This decrease is a result of cutting tool, tool holder, environment dissipating leftover heat and interrupting frictional heating. The sensor's capacity to detect temperatures in real-time is further confirmed by its rapid response during this phase. The common belief is that high temperatures are necessary for the development of titanium cutting. Since we mentioned this in the introduction, it is difficult to draw direct comparisons between this study's temperature measurements and those in the literature. As an example, temperatures ranging from 130℃ to 750℃ can be produced at high cutting speeds (80-90 m/min). Possible causes of these discrepancies include differences in tools, sensors' proximity to the edge, stability of the sensors, and stiffness of the tools themselves. According to this research, the observed temperatures are heavily influenced by distance of sensor from cutting edge. So that the shadow masks would not come loose when we deposited them, we placed our sensors about 1 mm from cutting edge. Although this placement is essential for patterning sensors, it may cause them to register lower temperatures than sensors located closer to the edge. The existing sensor location might not completely capture the peak temperatures that occur in this zone due to the strong friction and plastic deformation that occurs there.

3.5 Cutting Temperature Variation with Cutting Parameters

According to temperatures were measured in Fig. 4 while cutting titanium alloy by TiAlN sensor. The cutting circumstances were varied. Specifically, it shows how various cutting parameters affect the temperatures along the tool-workpiece interface.

The purpose of the studies was to determine how the cutting temperature changed in response to changes in low-pressure cooling, cutting speed, depth of cut and feed rate.

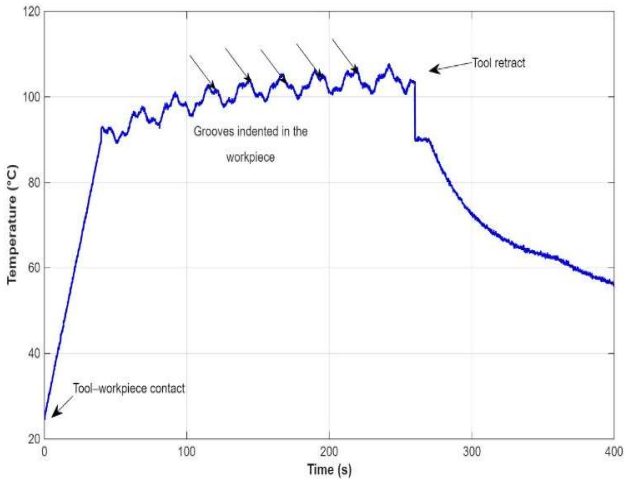

Fig. 3. Initial cutting test on Ti alloy with grooves

Changes in feed rate and depth of cut were depicted at Fig. 4(a) as temperature profiles. In the first three experiments, we see that maintaining a constant feed rate and raising depth of cut 1.0 to 1.5 mm leads to greater temperatures. The greater amount of material cut causes frictional heat, which in turn causes the temperature to rise. Temperature profiles remain mostly unaltered when feed rates are increased from 0.312 to 0.331 mm/rev and constant depth. This finding lends credence to the idea that feed rate is less of a factor in determining cutting temperature than depth of cut, which in turn reduces machining time. The impact of changing the depth while maintaining constant feed rate is seen at Fig. 4(b). Cutting temperature increases as depth cut increases 1.0 to 2.5 mm, as shown in Experiments 6-8 (Fig. 4(c)). It is well-known that enhanced frictional heating occurred as a result of higher cutting forces and more material deformation. By using fractal dimension features and a novel fractal index, distinct tool wear stages are identified efficiently, improving machining quality and reducing the need for prolonged titanium alloy tests [14]. Cutting at a faster rate causes more thermal loads at the cutting edge because less time is available for heat dissipation. Cutting at twice the normal speed and depth increases temperature by 40% and 30%, respectively, although increasing feed by 1.5 times only adds about 5-7%, highlighting the crucial role of speed and depth relative to feed. The effect of chilling on cutting temperature were seen at Fig. 4(d). Effectiveness of cooling at reducing cutting temperatures is demonstrated in Experiments 8 and 9. When dry cutting, the temperature peaks at around 190℃, but when cooling is applied, the temperature drops to around 110℃.

3.6 ZrAlN-Based Cutting Temperature Measurement

The temperature data taken by the ZrAlN film sensor during cutting of titanium alloy under various cutting circumstances are shown in Fig. 5. Through real-time temperature monitoring and tool-change demonstration, these tests sought to evaluate the ZrAlN performance. The "plug-and-play" capacity cutting tools integrated by thin-film is one of the breakthroughs emphasized by this study.

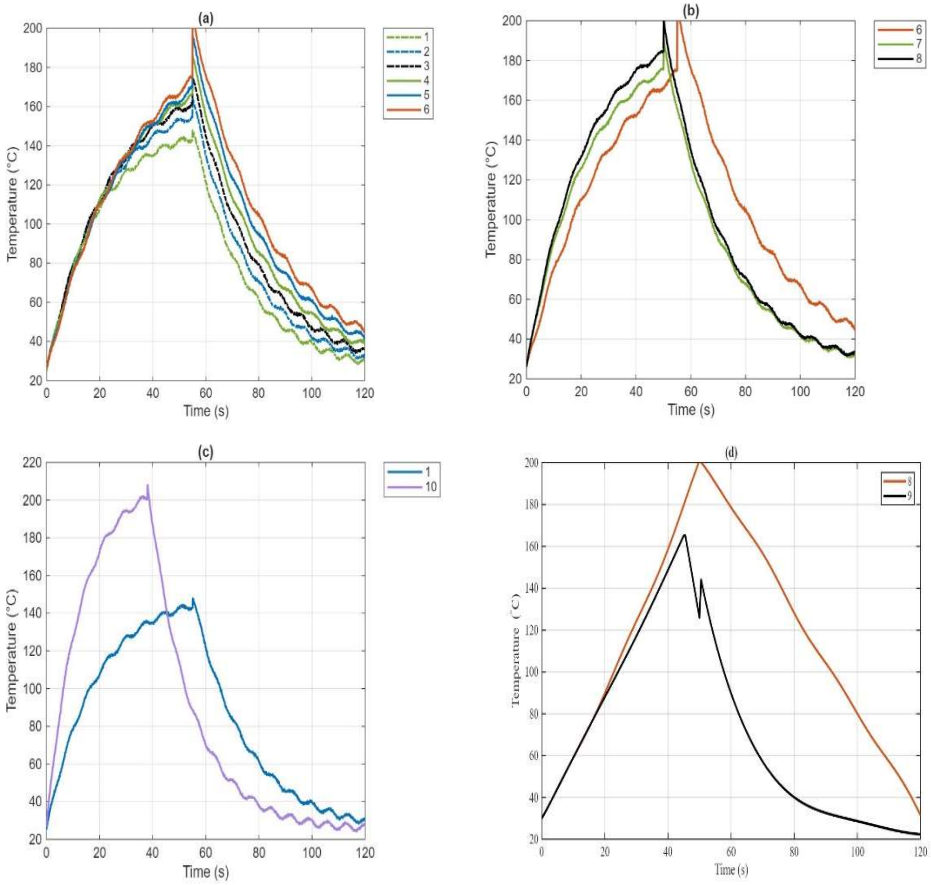

Fig. 4. Temperature measurements during titanium alloy cutting with TiAlN sensor under varying (a) ap, (b) f, (c) Vc, and (d) cooling conditions

It represents novel achievement at cutting sector. The different tools were without re-calibrate by changing the sensitivity of ZrAlN sensor at Arduino code. Simplifying process of tool replacement, this strategy bridges gap among industry and laboratory requirements. Under identical cutting settings, namely conditions 3, temperature profiles for tests 1-3 are shown in Fig. 5(a). In these tests, the reproducibility of temperature readings taken by ZrAlN sensor were controlled cutting settings was main objective. In all of these tests, the temperature profiles follow the same pattern: the tool heats up quickly at the beginning, then cools down as it pulls away from the workpiece. Similar to the TiAlN sensor's behavior seen in Fig. 5, this pattern follows suit. Take careful note of the variations in the temperature curve as the test progresses, particularly during test 3. A 45° taper is formed as the tool gets close to the lathe chuck because the cutting-edge angle of the holder is 45°. This means that if the tool holder is not immediately withdrawn, the depth of cut in consecutive cuts will be abruptly changed. An incident like this is seen in the inset of Fig. 5(a), where a big chip and the associated temperature curve peak are visible. This action further recognizes that cutting temperature were affected by depth of cut. Another factor to think about in cutting processes, particularly while turning, is cutting time, as seen in this image. The cutting temperature increases from 128 to 150ºC in 10 s due to the lack of a steady state, which is noticed during the cutting process.

The circumstances used in cutting tests 4–5, which were conducted under conditions 6; and cutting test 6, which was conducted under conditions 8 (Fig. 5(b)). Similar to curves 1, 2, and 3 in Fig. 5(a), test 4 and test 5 reveal similarity in the temperature curves when the cutting conditions are the same. The fact that the temperature curves are very similar throughout all of the experiments indicates that ZrAlN system is very repeatable and that sensors give very accurate temperature readings, even when subjected to very little changes in the cutting conditions or the positioning of the tool. Test 6's temperature peak at its conclusion lends credence to this hypothesis. The rapid response of the sensor is demonstrated by the peak temperature of over 320°C.

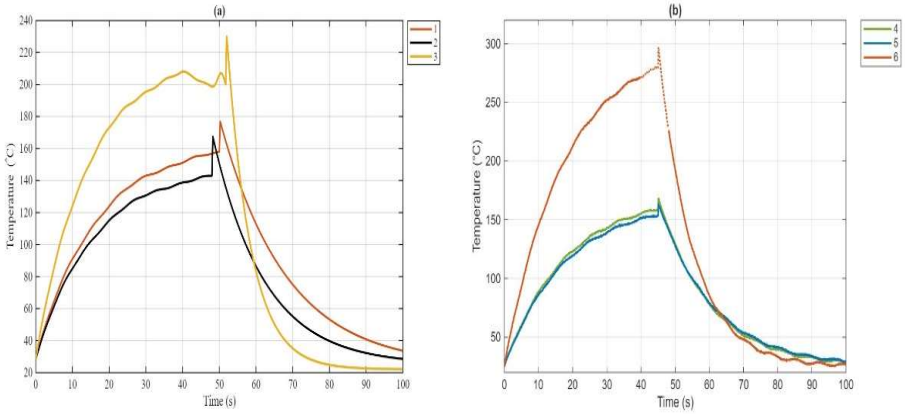

Fig. 5. Temperature measurements during titanium alloy cutting with TiAlN sensor: (a) tests 1–3 under condition 3; (b) tests 4–5 under condition 6 and test 6 under condition 8

3.7 Comparison of Sensor Performance

Fig. 6 shows the temperature profiles of TiAlN and ZrAlN sensors that were cut using the same parameters. The conditions shown in the bottom plot are 6, whereas the conditions shown in the top plot are 8. When cutting titanium alloy, these sensors show how comparable they are for real-time temperature monitoring. When subjected to identical cutting conditions, both sensors display identical temperature curve morphologies, suggesting a trustworthy calibration process. But the two sensors' maximum temperatures are different; the TiAlN recorded a temperature about 20°C higher. This small discrepancy will be explained by a combination of factors. The TiAlN sensor may be better calibrated using the β function. Secondly, when the shadow masks are manually placed during the sensor deposition process, there is a chance that slight positional deviations will occur. This could impact the exact location of sensor on tool's rake face, which in turn could cause temperature measurements to differ slightly. Finally, the design of the sensor could be a factor in the observed discrepancies. The meandering design of the TiAlN sensor may provide a more even dispersion of temperatures along the cutting edge. These findings provide more evidence that the two sensors can record the crucial cutting heat dynamics. When deciding which sensor is best suited for a certain task, it is essential to weigh benefits and drawbacks of all option. Because of its higher sensitivity, the ZrAlN sensor can replace the TiAlN one, which simplifies the electronics design by removing the requirement to amplify the signal. At temperatures greater than 300°C, the beta function calibration procedure seems to work better with the TiAlN sensor, which could lead to reduced measurement errors.

Despite the possibility of receiving sensors with high electrical resistance, the ZrAlN sensor's higher resistivity allows for simpler sensor designs.

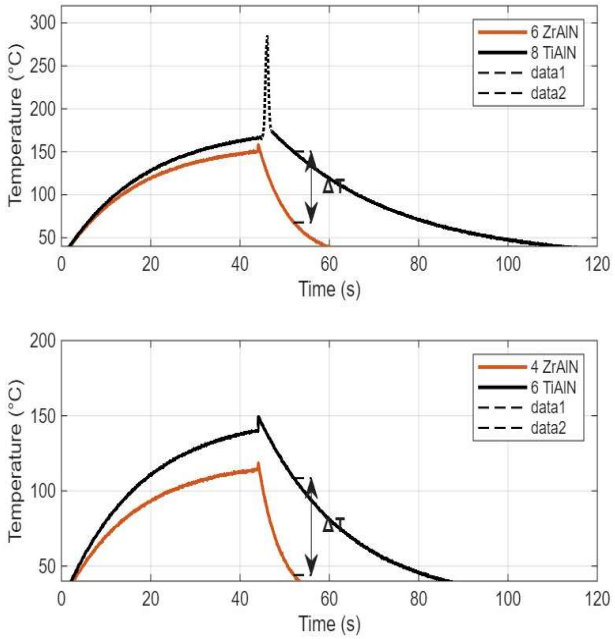

Fig. 6. Temperature profiles of TiAlN (bottom) and ZrAlN (top) sensors, with higher lathe speed for ZrAlN to match cutting speeds

3.8 Surface Topography and Wear Analysis of the Tool After Cutting

Fig. 7 shows an in-depth examination of topography of cutting tool's rake face, specifically in relation to the cutting edge. A three-dimensional topographical map of rake face is shown in center of image. The height changes across the surface are indicated by color scale on left. The sharp drop represents the tool's edge, and the vertical line represents a surface transition that corresponds to the edge of the sensor. At an x-dimension of around 0.8 mm, the sensor is spaced from the cutting edge. A comparable profile, this time along the y-axis, is shown in the top right inset. Sensor to cutting edge distance in y-direction is about 1.2 mm. It is to be assumed that the sensor-to-cutting-edge distances will differ slightly from Fig. 1 due to the shadow masks being manually positioned. After running the cutting tests, cutting tools with ZrAlN and TiAlN on rake surface produced a color profile. Three different kinds of wear are noticed on tool that has TiAlN sensor: crater wear abrasive wear and notch wear. The contact length—which were same as chip width and depth of cut of 2 mm, notch wear was localized to about 2.8 mm. As a result of localized material loss caused by high stresses and temperatures, this form of wear is probably accelerated when lengthy chips slide to left of tool holder. When chips are formed, workpiece and cutting edge come into frictional contact, leading to abrasive wear, which is most noticeable on the rake surface. By illuminating the degree of wear and revealing "stair" effect at multilayer coating is gradually exposed through the localized color index.

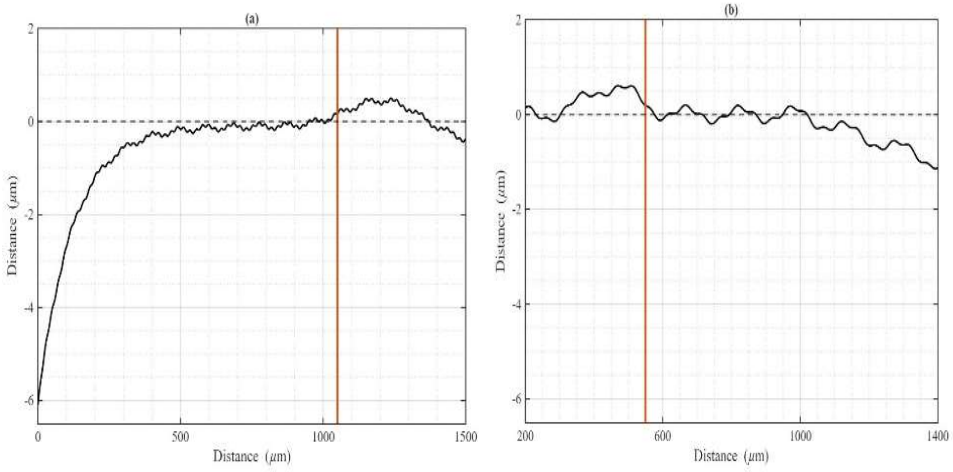

Fig. 7. TiAlN-coated tool edge with sensor edge

It is the tool-chip contact that undergoes abrasion and diffusion processes, leading to crater wear. Over time, the coating is worn away by abrasion, revealing the substrate. This allows the C and Co ions from WC-Co to diffuse into the chip, by reducing the edge strength. The high cutting speeds used, specifically cutting conditions 10 are likely to responsible for this form of wear that happens at high temperatures. Previous work wireless rotating tool holder system with integrated piezoelectric accelerometers was designed to capture real-time triaxial vibration during titanium machining. It effectively reduced attenuation and noise, showing high sensitivity and advancing smart machining applications in Industry 4.0 [15]. The sensor was about 680 μm away from center of crater, which is usually where the maximum temperatures occur. This placement aids in sensor protection, as mentioned before, but it restricts the precise cutting temperature assessment. Because of this restriction, the highest recorded temperature (210°C at 80 m/min) is misleading. Methods such as metal shadow masks that have been laser-trimmed are being considered as potential solutions to the present limitations. In our opinion, this method will allow us to place sensors in closer proximity to cutting zone, which will result in a more precise assessment of the cutting temperatures. The sensors' performance in industrial settings will be improved by this upgrade. Because of the uncontrolled ap seen in Fig. 5, abrasive wear goes well beyond length of cutting edge for depth of 2 mm. Based on length of exposed cutting edge, we may deduce that depth of cut approximately 8 mm at cutting temperature at 320°C. Furthermore, there are areas of chipping that have been identified. This could be due to chip curling against tool surface or brittle coating fracture. As anticipated, this instrument shows less wear than the one evaluated due to fact that it underwent fewer tests. This sensor differs slightly from the TiAlN sensor in that the distances are around 1.0 mm (y)and 1.2 mm (x). Variability at temperature comparisons among sensors, as seen at Fig. 6, could be caused by these variations. Therefore, in order to get the real cutting temperatures and do comparisons, the exact placement of the sensor is crucial.

4 Conclusions

This research represents a major step forward in temperature-controlled cutting (TCM) by incorporating conventional wear-resistant materials into cutting tools, with a focus on titanium alloys.

On cutting inserts, temperature sensors made of TiAlN and ZrAlN were applied in a multilayer coating and calibrated up to 750°C. The β sensitivities of the TiAlN and ZrAlN sensors were 112.4 and 928.6 K, correspondingly. Up to 420°C, the β function calibration was acceptable; however, the sensor's sensitivity sharply increased beyond that temperature, rendering it useless across the board. The impact of temperature on insulating characteristics of multilayer coating was thought to be responsible for this phenomenon. When deciding between TiAlN and ZrAlN, it is important to think about things like sensitivity, calibration fit, and design, even though both sensors captured the crucial thermal dynamics of cutting process. Because feed rate has less of an impact on cutting temperature than depth of cut and cutting speed, adjusting former two factors were more important for controlling cutting temperature. In comparison to modifying Vc or ap, cooling considerably lowers cutting temperatures. The study of the surface after cutting showed signs of crater wear, which implies placement of sensors is important for precise temperature readings because the highest temperature recorded were 210°C. Sensors that are positioned distant from the edge of cutting blade can miss the highest temperatures. Finally, this study offered a workable way for combining smart cutting tools with conventional tool holders, in an effort to connect laboratory testing with industrial temperature measurement applications. Machining operations are enhanced with the help of machine-to-tool connection made possible by real-time wireless temperature monitoring. Adjustments to cutting conditions can be made in real-time, which contributes to enhanced efficiency and decreased operational costs, and is in line with Industry 4.0 aims. Nevertheless, increasing the multilayer coating's electrical insulating qualities, perfecting shadow masks, and sensor location should be the focus of future effort.

References

1. R. Wang, Q. Song, Y. Peng, J. Qin, Z. Liu, Z. Liu, toward digital twins for high-performance manufacturing: tool wear monitoring in high-speed milling of thin-walled parts using domain knowledge. Journal of Manufacturing Processes. **88,** 102723 (2024). https://doi.org/10.1016/j.jmapro.2024.103381
2. D. Diaz Ocampo, D. Aubart, G. González, F. Zanger, M. Heizmann, Classification of the machine state in turning processes by using the acoustic emission. Journal of Manufacturing and Materials Processing. **18**, 289 (2024). https://doi.org/10.3390/jmmp18020289
3. K. Adithya, R. Girimurugan, Benefits of IoT in automated systems. Integration of Mechanical and Manufacturing Engineering with IoT: A Digital Transformation. 235 (2023).
4. L. Bernini, P. Albertelli, M. Monno, Mill condition monitoring based on instantaneous identification of specific force coefficients under variable cutting conditions. International Journal of Machine Tools and Manufacture. **185**, 109820 (2023). https://doi.org/10.1016/j.ijmachtools.2023.103923
5. T. Banda, V. L. Jauw, C. Li, A. A. Akhavan Farid, C. S. Lim, Multi-sectional SVD-based machine learning for imagery signal processing and tool wear prediction during CNC milling of Inconel 718. Journal of Intelligent Manufacturing. **132**, 4017 (2024). https://doi.org/10.1007/s10845-024-02276-5
6. B. Martins, C. Patacas, A. Cavaleiro, P. Faia, C.F.A. Alves, E. Carbo-Argibay, P.J. Ferreira, F. Fernandes, Zirconium aluminum nitride thin films for temperature sensing applications. Journal of Alloys and Compounds. **1013**, 178546 (2025). https://doi.org/10.1016/j.vacuum.2025.112233

7. B. Babu, S.K. Karthikeyan, B.H Babu, S. Nanthakumar, S. Sakthi, P. Vijayalakshmi, R. Girimurugan, E. Elango, M. Mathanbabu, Optimization on the Tool Parameters in Friction Stir Lap Joining of AA2219 by Response Surface Methodology. International Journal of Vehicle Structures & Systems. **16,** 663-670.
8. E. Aslan, Temperature prediction and performance comparison of permanent magnet synchronous motors using different machine learning techniques for early failure detection. Energies. **27**, (2025). https://doi.org/10.3390/en27010072
9. Z. Hai, Z. Su, K. Zhu, Y. Pan, S. Luo, Printed thick film resistance temperature detector for real-time tube furnace temperature monitoring. Sensors. **24**, 2999 (2024). https://doi.org/10.3390/s24103387
10. P. Ponnusamy, S. Seenivasan, G.B. Loganathan, D.M. Babu, A. Sivalingam, S. Nanthakumar, R. Girimurugan, Toolpath and Tool Design Innovations in Deformation Machining for Superior AA-7075 T6 Fins. In Journal of Physics: Conference Series. **2837,** 012060. https://doi.org/10.1088/1742-6596/2837/1/012060
11. Q. Yan, S. Chen, H. Shi, X. Wang, S. Meng, J. Li, Fabrication of polymer-derived SiBCN ceramic temperature sensor with excellent sensing performance. Ceramics International. **43**, 7373 (2023). https://doi.org/10.1016/j.ceramint.2023.7373
12. H. Liu, W. Dong, X. Sun, S. Wang, W. Li, Performance of Fe-Ga alloy rotational vibration energy harvester with centrifugal softening. Smart Materials and Structures. **31**, 065008 (2022). https://doi.org/10.1088/1361-665X/ac653f
13. M. Chinnasamy, R. Rathanasamy, G. V. Gobinath, P. Paramasivam, S. K. Jaganathan, A frontier statistical approach towards online tool condition monitoring and optimization for dry turning operation of Sae 1015 steel. International Journal of Advanced Manufacturing Technology. **66**, 901 (2021). https://doi.org/10.1007/s00170-021-07182-9
14. G. Greczynski, S. Mráz, M. Hans, J. Lu, L. Hultman, J. M. Schneider, Control over the phase formation in metastable transition metal nitride thin films by tuning the Al+ subplantation depth. Materials Advances. **9**, 17 (2019). https://doi.org/10.1039/C9MA00456A
15. M. Jamshidi, X. Rimpault, M. Bałaziński, J.-F. Châtelain, Fractal analysis implementation for tool wear monitoring based on cutting force signals during CFRP/titanium stack machining. Journal of Manufacturing Processes. **106**, 3859 (2020). https://doi.org/10.1016/j.jmapro.2020.08.017